Got meat?
The mechanical signature of plant-based and animal meat

Skyler R. St. Pierre[1], Ethan C. Darwin[1], Divya Adil[1], Magaly C. Aviles[1], Archer Date[1], Reese A. Dunne[1], Yanav Lall[1], María Parra Vallecillo[1], Valerie A. Perez Medina[1], Kevin Linka[2], Marc E. Levenston[1], Ellen Kuhl[1*]

[1] Department of Mechanical Engineering, Stanford University, California, United States.
[2] Institute of Applied Mechanics, RWTH Aachen, Aachen, Germany.

*Corresponding author(s). E-mail(s): ekuhl@stanford.edu;

Abstract

Eating less meat is associated with a healthier body and planet. Yet, we remain reluctant to switch to a plant-based diet, largely due to the sensory experience of plant-based meat. The gold standard test to analyze the texture of food is the double mechanical compression test, but it only characterizes one-dimensional behavior. Here we use tension, compression, and shear tests along with a constitutive neural network to automatically characterize the mechanics of eight plant- and animal-based meats across the entire three-dimensional spectrum. We discover that plant-based sausage and hotdog, with stiffnesses from 35.3kPa to 106.3kPa, successfully mimic the behavior of their animal counterparts, with stiffnesses from 26.8kPa to 115.5kPa, while tofurky with 167.9kPa to 224.5kPa is twice as stiff, and tofu with 22.3kPa to 34.0kPa is twice as soft. Strikingly, the more processed the product–with more additives and ingredients–the more complex the mechanics: The best model for the softest, simplest, and oldest product, plain tofu, is the simplest, the classical neo Hooke model; the best model for the stiffest products, tofurky and plant sausage, is the popular Mooney Rivlin model; the best models for all highly processed real meat products are more complex with quadratic and exponential terms. Interestingly, all animal products are stiffer in tension than in compression, while all plant-based products, except for extra firm tofu, are stiffer in compression. Our results suggest that probing the fully three-dimensional mechanics of plant- and animal-based meats is critical to understand subtle differences in texture that may result in a different perception of taste. We anticipate our models to be a first step towards using generative artificial intelligence to scientifically reverse-engineer formulas for plant-based meat products with customer-friendly tunable properties.

Our data and code are freely available at https://github.com/LivingMatterLab/CANN

Keywords: plant-based, meat, material properties, processed food, mechanics

Current meat production is inefficient and unsustainable [1]. It is a key driver for climate change, environmental degradation, and antibiotic resistance [2]. A common strategy to quantify the efficiency of animal meat is to compare energy out versus energy in, and protein out versus protein in [3]. On a global average, energy conversion efficiencies range from 11% for poultry to 10% for pork, and 1% for beef and sheep; while protein conversion efficiencies range from 20% for poultry to 15% for pork, 4% for beef, and 3% for sheep [4]. In other words, cattle are a particularly inefficient conversion system: They convert only one percent of the gross energy and four percent of the protein in their feed to energy and protein in edible beef [5].

At the same time, the consumption of a kilogram of beef is estimated to have the same greenhouse gas emission impact as driving 1.172km in a

gas-fueled passenger car [6]. On a global average, the estimated greenhouse gas emission in kg carbon dioxide equivalents per kg food varies from 100 for beef to 40 for sheep, 12 for pork, and 10 for poultry, while it is only 3 for tofu [7]. These alarming numbers underscore that the global food system is a major source of greenhouse gas emissions [8]. In fact, experts estimate that it will be critical to change the global food system to meet the Paris Agreement of limiting the increase in global temperature to 1.5 to 2.0°C above its pre-industrial levels [9].

Equally concerning is the increasing use of antimicrobials in food animals to promote growth, increase health, and maintain food safety [10]. On a global average, the estimated annual consumption of antimicrobials per kilogram of animal meat ranges from 172mg for pigs, to 148mg for chicken, and 45mg for cattle [11]. These practices contribute to the spread of drug-resistant pathogens in both livestock and humans. Based on current trends, medical experts expect 10 million annual deaths from antimicrobial resistance in 2050, a 14-fold increase over current deaths [12]. Beyond these global concerns, eating red and processed meat is associated with an increased individual risks of colorectoral cancer, chronic kidney disease, type 2 diabetes, and cardiovascular disease [13]. Taken together, it is becoming increasingly clear that a shift towards consuming less meat is needed for the health of the planet and people [1]

Plant-based meat products are alternatives to animal meat that are produced directly from plants [14]. The fundamental idea is to avoid using animals to convert vegetation into meat. Recent studies suggest that plant-based meat products have a 50% lower environmental impact than animal meat [15]; yet, their adoption into our diets remains low [16]. Although more and more people are intrigued by a flexitarian diet and intentionally reduce their animal meat intake, most of us do not eliminate meat entirely [17]. A recent consumer survey revealed that in the United States, only one third of participants were very or extremely likely to buy plant-based meat products [18]. This reluctancy supports the emerging view that the key to a more sustainable food system is not to convince consumers to give up the foods they like [1]; instead, scientists should focus on creating plant-based products that taste the same or better than animal meat [19]. In fact, our sensory experience–including taste and texture–is one of the most important reasons for choosing which product we eat [16]. But how can we reliably and reproducibly quantify and compare the texture of different meat products?

According to its widely-accepted definition, texture is the sensory and functional manifestation of the structural, mechanical, and surface properties of food. [20]. *Sensory manifestation* has been the focus of numerous food texture surveys [21], but their results vary greatly by personal preference, subjective interpretation, cultural background, sensory ability, lack of standardization, and various external factors [16]. *Functional manifestation* has traditionally been quantified by texture profile analysis [22], using a double mechanical compression test [23]. This method is quantitative, objective, and standardized [24], but only provides insights into the one-dimensional compressive behavior of the product [25]. If plant-based meat products are to mimic the true textural properties of animal meat, how can we comprehensively characterize the fully three-dimensional mechanics of artificial and real meat? And, ultimately, how can we use this knowledge to inform the design of more animal-like meat alternatives?

The objective of our study is to understand the mechanical signatures of artificial and real meat. Animal meat consists of muscle, connective tissue, fat, and water, and is dominated by its anisotropic microstructure [26]. In contrast, most plant-based meats are made of soy-, wheat-, or pea-based proteins, they have no pronounced fibers, and are generally isotropic [14]. To unify our comparison, we focus on processed meat products–plant-based and real sausage and hotdog–and assume that these products are homogeneous and isotropic. For comparison, we also characterize processed plant-based and real turkey, and two plain soy protein products, extra firm and firm tofu. We systematically compare all eight products through standardized mechanical tension, compression, and shear tests [27], combined with automated model discovery to discover the best models and parameters for each product [28]. To accelerate discovery and innovation in plant-based food technologies [1], we share all raw data, methods, algorithms, and results on a public open source discovery platform.

Results

Mechanical testing. We mechanically tested eight products, five plant-based, tofurky, plant sausage, plant hotdog, extra firm tofu, and firm tofu, and three animal-based, spam turkey, real sausage, and real hotdog. Table 1 summarizes the brand name, manufacturer, and list of ingredients of all eight products. For each product, we performed tension, compression, and shear tests on at least $n = 5$ samples per testing mode. Table 2 in the Extended Data summarizes the means ± standard error of the means for all eight products and all three tests. Figure 1 shows the resulting stress-stretch

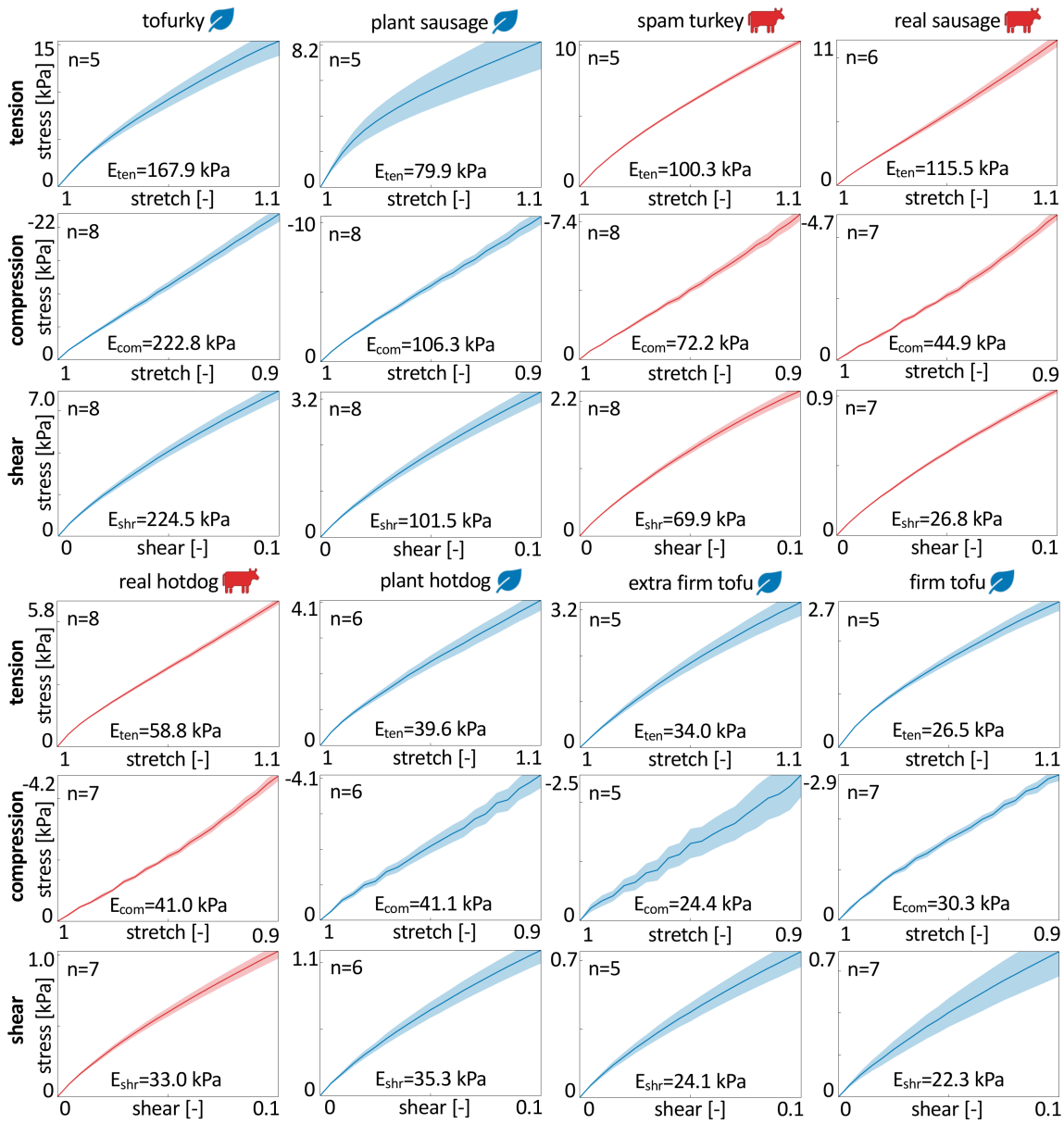

Fig. 1 Mechanical testing. Tofurky, plant sausage, spam turkey, real sausage, real hotdog, plant hotdog, extra firm tofu, and firm tofu tested in tension, compression, and shear. Stresses are reported as means ± standard error of the means of n samples tested in the ranges $1.0 \leq \lambda \leq 1.1$ for tension, $0.9 \leq \lambda \leq 1.0$ for compression, and $0.0 \leq \gamma \leq 0.1$ for shear. Each plot reports the sample size n and the stiffness, E_{ten}, E_{com}, E_{shr}. Plant-based products are colored in blue, animal-based products in red.

and shear stress-strain curves with the plant-based products in blue and animal-based products in red. The small standard error, highlighted as the shaded region around the mean, reveals that there is little sample-to-sample variation and that our mechanical tests are solidly reproducible. Notably, tofurky displays by far the stiffest response, followed by plant sausage, the three animal-based products, spam turkey, real sausage, and real hotdog, and then plant hotdog, extrafirm tofu, and firm tofu. Interestingly, the plant-based products, plant sausage and plant hotdog, display similar mechanical properties as their animal-based counterparts, real sausage and real hotdog, whereas the two tofu products are notably softer.

Mechanical signatures. We extract the mechanical signatures of all eight products from Table 2 in the Extended Data and directly compare the tensile, compressive, and shear stiffnesses, the peak tensile stresses and stretches, and the tension-compression asymmetry of the eight products in Figure 2 and in Table 1. Plant-based products are colored in blue,

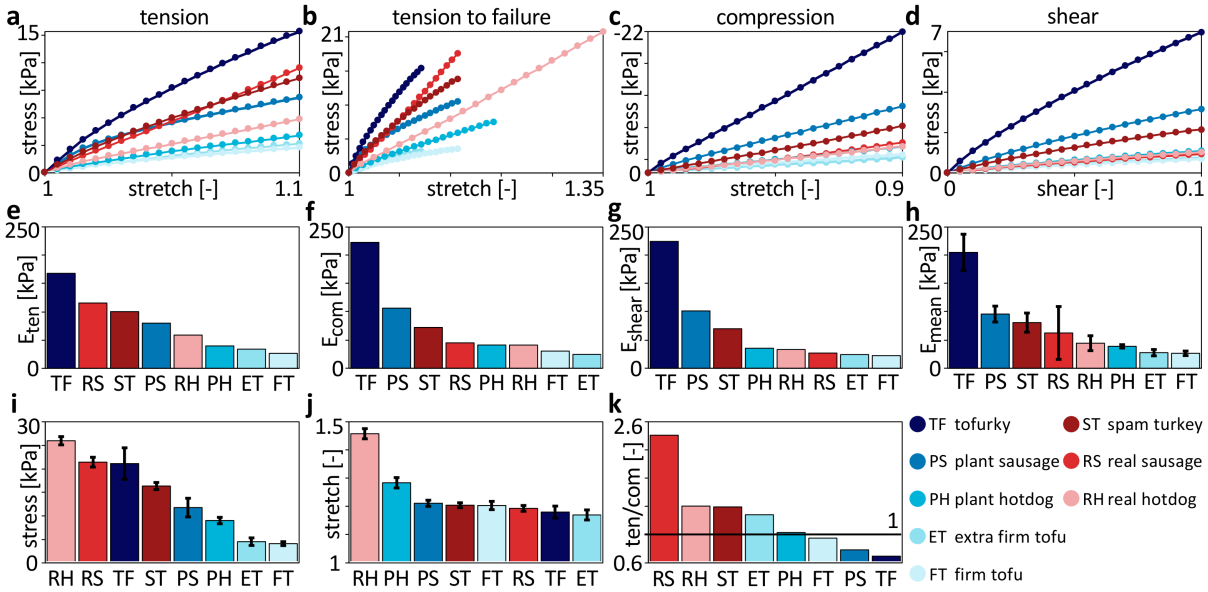

Fig. 2 Mechanical signatures. Tofurky, plant sausage, spam turkey, real sausage, real hotdog, plant hotdog, extra firm tofu, and firm tofu characterized in tension, compression, and shear. **a.** Tensile stress-stretch curves up to +10% stretch. **b.** Compressive stress-stretch curves up to −10% stretch. **c.** Shear stress-strain curves up to 10% shear strain. **d.** Tensile stress-stretch curves up to failure. **e.** Tensile stiffness E_{ten}. **f.** Compressive stiffness E_{com}. **g.** Shear stiffness E_{shear}. **h.** Mean stiffness E_{mean} with standard deviation. **i.** Peak tensile stress, mean and standard deviation. **j.** Peak tensile stretch, mean and standard deviation. **k.** Tension-compression asymmetry in stress at 10% stretch. The black line indicates tension-compression symmetry, products above the line have a greater tensile stress and products below the line have a greater compressive stress. The legend shows the two-letter keys and colors that correspond to each product with plant-based products in blue and animal-based products in red.

animal-based products in red, with darker colors indicating a stiffer response across all testing modes. Figure 2 **a** shows the tensile stress-stretch curves for stretches up to +10%. In addition, we test all tensile samples to failure, where we define failure as a notable drop in the stress response, and plot the tensile stress-stretch curves *before* failure occurs in Figure 2 **b**. Both tofurky and extra firm tofu exhibit failure slightly above 10% stretch, while all other products stretch up to 15%–20% without failing. Real hotdog stretches the furthest, up to 35%, and reaches the largest peak stress. Figures 2 **c** and 2 **d** show the compressive stress-stretches curves for stretches up to -10%, and the shear stress-strain curves for shear strains up to 10%. Clearly, across the entire top row, in all three modes, tofurky is the stiffest, and the two tofu products are the softest. From the tension, compression, and shear curves in Figures 2 **b**-**d**, we extract the linear elastic modulus using linear regression and report it as the tensile, compressive, and shear stiffnesses E_{ten}, E_{com}, E_{shr} in Figures 2 **e**-**g**, and as the mean stiffness E_{mean} ± standard deviation across all three modes in Figure 2 **h**. Across all three modes, tofurky with a stiffness of 205.1±32.2 kPa is by far the stiffest product. In fact, it is more than twice as stiff as the second and third products, plant sausage with 95.9±14.1 kPa and spam turkey with 80.8±16. the kPa. The two tofu products are consistently the softest products across all three loading modes, where extra firm tofu with a stiffness of 27.5±5.6 kPa is slightly stiffer than firm tofu with 26.4±4.0 kPa. From the tension-to-failure curves in Figure 2 **b**, we extract the peak tensile stress in Figure 2 **i** and the peak tensile stretch in Figure 2 **j**. Interestingly, real hotdog displays the largest peak stress and stretch. Tofurky and real sausage both have high peak stresses, but much lower peak stretches. Extra firm and firm tofu have by far the lowest peak stresses. Figure 2 **k** shows the tension-compression asymmetry at ±10% stretch. The black line indicates tension-compression symmetry; a value larger than one means that the product is stiffer in tension than in compression, and a value smaller than one means the opposite. Strikingly, all three real meats products display a larger stiffness in tension than in compression. Real sausage shows the largest asymmetry with 2.41, followed by real hotdog with 1.41 and spam turkey with 1.39. The only plant-based product with a comparable tension-compression asymmetry is extra firm tofu with 1.29. Plant hotdog with 1.03, firm tofu with 0.95, plant sausage with 0.79 and tofurky with 0.70, all display either close to no asymmetry or a larger stiffness in compression than in tension.

Model discovery. The mechanical signatures in

Table 1 Real and artificial meat products. Products; brands; ingredients; stiffnesses in tension, compression, shear, and mean stiffness; peak strain and stress; discovered best-in-class one- and two-term models, parameters, and goodness of fit.

	TF Tofurky	**PS Plant Sausage**	**ST Spam Turkey**	**RS Real Sausage**
brand	Ham-Style Roast Tofurky Hood River, OR	Vegan Frankfurter Sausage Field Roast Seattle, WA	Spam Oven Roasted Turkey Spam, Hormel Foods Co Austin, MN	Turkey Polska Kielbasa Hallshire Farm New London, WI
ingredients	water, vital wheat gluten, tofu (water, soybeans, magnesium chloride, calcium chloride), expeller pressed canola oil; contains 2% or less: sea salt, spices, granulated garlic, cane sugar, natural flavors, natural smoke flavor, color, oat fiber	filtered water, vital wheat gluten, expeller pressed safflower oil, organic expeller pressed palm fruit oil, barley malt, naturally flavored yeast extract, tomato paste, apple cider vinegar, paprika, sea salt, onions, spices, whole wheat flour	white turkey, turkey broth, salt, modified potato starch, sugar, dextrose, sodium nitrite	turkey, mechanically separated turkey, water, corn syrup; contains 2% or less: natural flavors, salt, dextrose, oat fiber, modified corn starch, monosodium glutamate, sodium erythorbate, yeast extract, sodium nitrite
stiffness	$E_{\text{ten}} = 167.9$ kPa $E_{\text{com}} = 222.8$ kPa $E_{\text{shr}} = 224.5$ kPa $E_{\text{mean}} = 205.1 \pm 32.2$ kPa	$E_{\text{ten}} = 79.9$ kPa $E_{\text{com}} = 106.3$ kPa $E_{\text{shr}} = 101.5$ kPa $E_{\text{mean}} = 95.9 \pm 14.1$ kPa	$E_{\text{ten}} = 100.3$ kPa $E_{\text{com}} = 72.2$ kPa $E_{\text{shr}} = 69.9$ kPa $E_{\text{mean}} = 80.8 \pm 16.9$ kPa	$E_{\text{ten}} = 115.5$ kPa $E_{\text{com}} = 44.9$ kPa $E_{\text{shr}} = 26.8$ kPa $E_{\text{mean}} = 62.4 \pm 46.8$ kPa
peak	$\varepsilon = 10\%$, $\sigma = 15.4$ kPa	$\varepsilon = 15\%$, $\sigma = 10.5$ kPa	$\varepsilon = 15\%$, $\sigma = 13.8$ kPa	$\varepsilon = 15\%$, $\sigma = 17.6$ kPa
one-term model	$w_5 = 33.08$ kPa $R^2 = 0.9810$	$w_5 = 16.01$ kPa $R^2 = 0.9588$	$w_2 = 3.21$ kPa, $w_2^* = 3.92$ $R^2 = 0.8366$	$w_2 = 0.42$ kPa, $w_2^* = 16.01$ $R^2 = 0.5310$
two-term model	$w_1 = 12.27$ kPa $w_5 = 20.94$ kPa $R^2 = 0.9799$	$w_1 = 6.56$ kPa $w_5 = 9.34$ kPa $R^2 = 0.9624$	$w_1 = 11.33$ kPa $w_3 = 51.77$ kPa $R^2 = 0.8464$	$w_1 = 3.63$ kPa $w_4 = 11.85$ kPa, $w_4^* = 11.83$ $R^2 = 0.5311$
	RH real hotdog	**PH plant hotdog**	**ET extra firm tofu**	**FT firm tofu**
brand	Classic Uncured Wiener Oscar Mayer, Kraft Heinz Co Chicago, IL	Signature Stadium Hot Dog Field Roast Seattle, WA	Organic Tofu Extra Firm House Foods Garden Grove, CA	Organic Firm Tofu 365 by Whole Foods Market Austin, TX
ingredients	mechanically separated chicken, mechanically separated turkey, pork, water, corn syrup; contains 2% or less: salt, sodium phosphate, potassium chloride, sodium diacetate, sodium benzoate, sodium ascorbate, flavor, sodium nitrate	water, soybean oil, pea protein, potato starch, contains 2% or less: methylcellulose, carrageenan, sea salt, brown rice protein, faba beam protein, garlic powder, beet powder, cane sugar, natural flavor, wheat gluten, soy protein, konjac flour, potassium chloride, xanthan gum, spices, paprika, red rice flour	water, organic soybeans, calcium sulfate, calcium chloride	water, organic soybeans, calcium sulfate, magnesium chloride
stiffness	$E_{\text{ten}} = 58.8$ kPa $E_{\text{com}} = 41.0$ kPa $E_{\text{shr}} = 33.0$ kPa $E_{\text{mean}} = 44.3 \pm 13.2$ kPa	$E_{\text{ten}} = 39.6$ kPa $E_{\text{com}} = 41.1$ kPa $E_{\text{shr}} = 35.3$ kPa $E_{\text{mean}} = 38.7 \pm 3.0$ kPa	$E_{\text{ten}} = 34.0$ kPa $E_{\text{com}} = 24.4$ kPa $E_{\text{shr}} = 24.1$ kPa $E_{\text{mean}} = 27.5 \pm 5.6$ kPa	$E_{\text{ten}} = 26.5$ kPa $E_{\text{com}} = 30.3$ kPa $E_{\text{shr}} = 22.3$ kPa $E_{\text{mean}} = 26.4 \pm 4.0$ kPa
peak	$\varepsilon = 35\%$, $\sigma = 20.8$ kPa	$\varepsilon = 20\%$, $\sigma = 7.5$ kPa	$\varepsilon = 10\%$, $\sigma = 3.2$ kPa	$\varepsilon = 15\%$, $\sigma = 3.5$ kPa
one-term model	$w_2 = 2.55$ kPa, $w_2^* = 2.59$ $R^2 = 0.9308$	$w_2 = 2.61$ kPa, $w_2^* = 2.35$ $R^2 = 0.9743$	$w_1 = 4.42$ kPa $R^2 = 0.8318$	$w_1 = 4.51$ kPa $R^2 = 0.9494$
two-term model	$w_1 = 5.80$ kPa $w_7 = 22.83$ kPa $R^2 = 0.9471$	$w_1 = 6.22$ kPa $w_3 = 7.25$ kPa $R^2 = 0.9747$	$w_1 = 4.42$ kPa – $R^2 = 0.8318$	$w_1 = 4.51$ kPa – $R^2 = 0.9494$

Figure 2 provide valuable first insight into the material behavior of the plant- and animal-based products. However, these signatures are only one-dimensional, and cannot predict the complex material behavior of the eight products in real three-dimensional chewing. We now discover the fully three-dimensional best-in-class one- and two-term models for all eight products using the constitutive neural network in Figure 6 in the Extended Data. Figure 3 summarizes the results for the eight different meat products in terms of the best one- and two-term models made up of eight functional building blocks: linear, exponential linear, quadratic, and exponential quadratic in the first and second strain invariants I_1 and I_2. The color code indicates the quality of fit to the tension, compression, and shear data from Table 2 in the Extended Data, with dark blue indicating the best fit and dark red the worst. Here we use the full tension data, not just the 10% stretch, after comparing the real hotdog model discovery with tensile stretches up to 10% versus 35% in the Extended Data Figure 8. We observe that, with the entire tension regime, the error plot becomes more non-uniform, and the best-in-class models are easier to delineate.

For the best-in-class one-term models that correspond to the bluest most term on the diagonals of Figure 3, we discover three prominent soft matter models: the linear second invariant Blatz Ko model [29], $w_5[\,I_2 - 3\,]$, for tofurkey and plant sausage, the exponential linear first invariant Demiray model [30], $w_2[\exp(w_2^*\,[\,I_1 - 3\,]) - 1]$, for spam turkey, real sausage, real hotdog, and plant hotdog, and the linear first invariant neo Hooke model [31], $w_1[\,I_1 - 3\,]$, for extra firm tofu and firm tofu, with the following

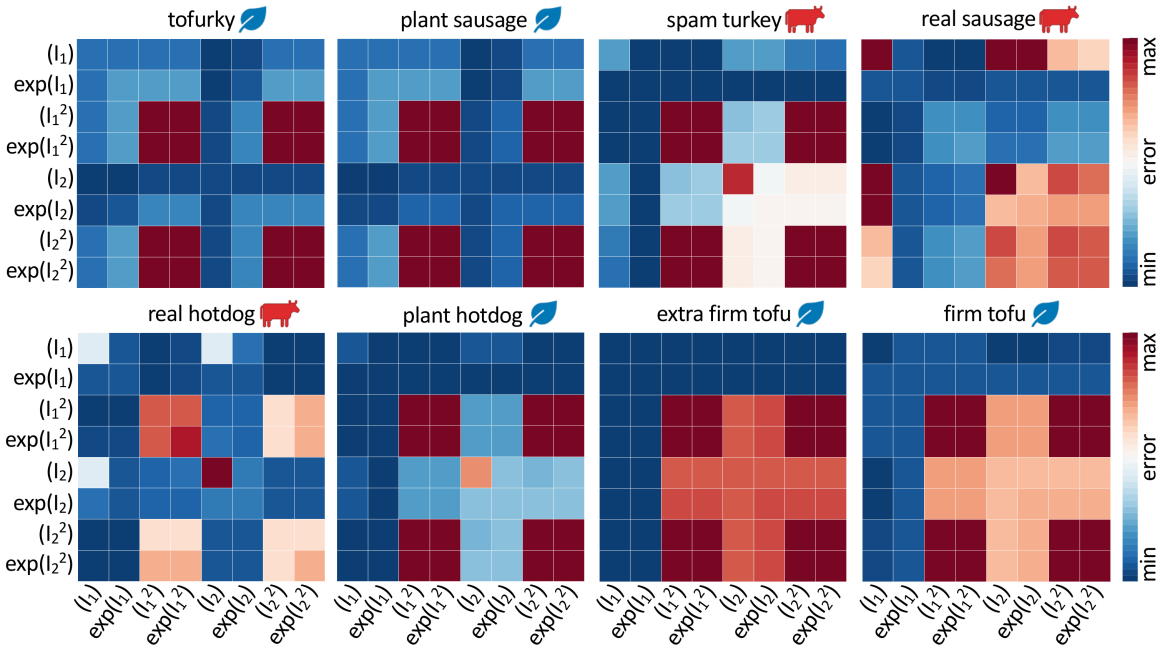

Fig. 3 Model discovery. Discovered one-term models, on the diagonal, and two-term models, off-diagonal, for tofurky, plant sausage, spam turkey, real sausage, real hotdog, plant hotdog, extra firm tofu, and firm tofu. All models are made up of eight functional building blocks: linear, exponential linear, quadratic, and exponential quadratic terms of the first and second strain invariants I_1 and I_2. The color code indicates the quality of fit to the tension, compression, and shear data from Table 2 in the Extended Data, ranging from dark blue, best fit, to dark red, worst fit.

best-fit parameters,

$$
\begin{aligned}
&\textbf{TF} && \psi = 22.08\,[\,I_2 - 3\,] \\
&\textbf{PS} && \psi = 16.01\,[\,I_2 - 3\,] \\
&\textbf{ST} && \psi = 3.21\,[\,\exp(3.92\,[\,I_1 - 3\,]) - 1] \\
&\textbf{RS} && \psi = 0.42\,[\,\exp(16.01\,[\,I_1 - 3\,]) - 1] \\
&\textbf{RH} && \psi = 2.55\,[\,\exp(2.59\,[\,I_1 - 3\,]) - 1] \\
&\textbf{PH} && \psi = 2.61\,[\,\exp(2.35\,[\,I_1 - 3\,]) - 1] \\
&\textbf{ET} && \psi = 4.42\,[\,I_1 - 3\,] \\
&\textbf{FT} && \psi = 4.51\,[\,I_1 - 3\,]\,.
\end{aligned}
$$

Notably, none of the quadratic terms, I_1^2, $\exp(I_1^2)$, I_2^2, $\exp(I_2^2)$, describe the material behavior well, as we conclude from the red squares on the eight diagonals in Figure 3.

For the best-in-class two-term models that correspond to the bluest most term overall, we discover the linear first and second invariant Mooney Rivlin model [32, 33], $w_1[\,I_1 - 3\,] + w_5[\,I_2 - 3\,]$, for tofurkey and plant sausage, the linear and quadratic first invariant model, $w_1[\,I_1 - 3\,] + w_3[\,I_1 - 3\,]^2$, for spam turkey and plant-based hotdog, the linear and exponential quadratic first invariant model, $w_1[\,I_1 - 3\,] + w_4[\exp(w_4^*\,[\,I_2 - 3\,]^2) - 1]$, for real sausage, the linear first and quadratic second invariant model, $w_1[\,I_1 - 3\,] + w_7[\,I_2 - 3\,]^2$, for real hotdog, and the linear first invariant neo Hooke model [31], $w_1[\,I_1 - 3\,]$, for extra firm tofu and firm tofu, with the following best-fit parameters,

$$
\begin{aligned}
&\textbf{TF} && \psi = 12.27\,[\,I_1 - 3\,] + 20.94\,[\,I_2 - 3\,] \\
&\textbf{PS} && \psi = 6.56\,[\,I_1 - 3\,] + 9.34\,[\,I_2 - 3\,] \\
&\textbf{ST} && \psi = 11.33\,[\,I_1 - 3\,] + 51.77\,[\,I_1 - 3\,]^2 \\
&\textbf{RS} && \psi = 3.63\,[\,I_1 - 3\,] + 11.85\,[\exp(11.83[\,I_2 - 3\,]^2) - 1] \\
&\textbf{RH} && \psi = 5.80\,[\,I_1 - 3\,] + 22.83\,[\,I_2 - 3\,]^2 \\
&\textbf{PH} && \psi = 6.22\,[\,I_1 - 3\,] + 7.25\,[\,I_1 - 3\,]^2 \\
&\textbf{ET} && \psi = 4.42\,[\,I_1 - 3\,] \\
&\textbf{FT} && \psi = 4.51\,[\,I_1 - 3\,]
\end{aligned}
$$

Notably, all eight models contain the classical linear first invariant neo Hooke term [31], $[\,I_1 - 3\,]$. All eight products, except for real sausage, show the same four dark red corners patterns, which indicate that the I_1^2, $\exp(I_1^2)$, I_2^2, $\exp(I_2^2)$ terms provide the worst fit to the data. From the nearly identical error maps, we conclude that tofurky and plant sausage have a similar mechanical behavior, and so do plant hotdog, extra firm tofu, and firm tofu. In contrast, the three animal-based products, spam turkey, real sausage, and real hotdog, have the most distinct error maps, suggesting that their mechanical behavior is notably different. Interestingly, for both tofu products, the model fit does not improve by adding a second term, and their best-in-class two-term model is identical to their best-in-class one-term model: the classical neo Hooke model [31].

To visualize how well these discovered models

approximate to our mechanical tests, we color-code the stress contributions of the individual terms and illustrate them together with the raw data in Figure 7 of the Extended Data. The eight columns correspond to each of the eight products, and the rows represent the tension, compression, and shear experiments. The dark red term that consistently appears in all eight models is the classical linear first invariant neo Hooke term [31], $w_1\,[\,I_1 - 3\,]$. In addition, both tofurky and plant sausage have a turqouise linear second invariant Blatz Ko term [29], $w_5\,[\,I_2 - 3\,]$, spam turkey and plant hotdog have an orange quadratic first invariant term, $w_3\,[\,I_1 - 3\,]^2$, real sausage has a yellow exponential quadratic first invariant term, $w_4\,\exp(w_4^*[\,I_1 - 3\,]^2) - 1$, real hotdog has a blue quadratic second invariant term, $w_7\,[\,I_2 - 3\,]^2$, and extra firm tofu and firm tofu have no additional second term.

Table 1 summarizes the discovered best-in-class one- and two-term models and parameters. For the Mooney Rivlin type models, we can directly translate the network weights into the shear modulus μ using $\mu = 2\,w_1 + 2\,w_5$. So, the shear moduli of the two stiffest products, tofurky and plant sausage, are 66.42 kPa and 31.80 kPa, and the shear moduli of the two softest products, extra firm and firm tofu, are 8.84 kPa and 9.04 kPa. Interestingly, the shear modulus for firm tofu is slightly larger than for extra firm tofu. We can translate these shear moduli μ into Young's moduli, $E = 2\,[1 + \nu]\,\mu$, by assuming a Poisson's ratio of $\nu = 0.5$ for perfect incompressibility, and we find Young's moduli of 199.25 kPa, 95.40 kPa, 26.53 kPa, and 27.08 kPa for tofurky, plant sausage, extra firm tofu, and firm tofu. These values are in excellent agreement with the mean stiffnesses from our linear regression in Figure 2 **h**, 205.09 kPa, 95.89 kPa, 27.48 kPa, and 26.35 kPa for tofurky, plant sausage, extra firm tofu, and firm tofu. For the other four products, spam turkey, real sausage, real hotdog, and plant hotdog, we discover novel constitutive models with quadratic or exponential terms that do not directly translate into Young's moduli. Interestingly, all three animal-based products are in this group, indicating that real meat, even when highly processed, has a more complex mechanical behavior than plant-based meat alternatives.

Discussion

We tested five plant-based products, tofurky, plant sausage, plant hotdog, extra firm and firm tofu, and three animal-based products, spam turkey, real sausage, and real hotdog, in tension, compression, and shear. We focused on highly processed artificial and real meats, assuming that all products are nearly isotropic and homogeneous, and, as our study confirms, easy and reproducibly to test. We performed a total of 157 mechanical tests and 288 neural network simulations. Our goal was to probe *to which extent do plant-based meat products mimic the mechanical signature of animal-based meat*, not just in a double-compression texture profiling analysis, but across the entire three-dimensional spectrum. While our study is limited by our assumption of isotropy and by probing raw products at room temperature, it uncovers several interesting and unexpected results:

Plant-based sausage and hotdog succeed in mimicking the mechanical signature of their animal-based counterparts. Our results confirm that our mechanical tension, compression, and shear tests are well reproducible with narrow errors and standard deviations, as we conclude from Figure 1 and Table 1. From the mean tension, compression, and shear curves in Figures 2 **a,b,c,d**, we conclude that plant sausage and plant hotdog consistently lie in the middle range of all eight products, and place closer to the three animal meats than the two tofu products. When comparing at the stiffnesses in Figures 2 **e,f,g,h**, plant sausage and plant hotdog range from $E = 35.3\,\text{kPa}$ to $E = 106.3\,\text{kPa}$ and fall in a comparable category as real sausage and real hotdog ranging from $E = 26.8\,\text{kPa}$ to $E = 115.5\,\text{kPa}$. In contrast, tofurky ranges from $E = 167.9\,\text{kPa}$ to $E = 224.5\,\text{kPa}$ and is consistently more than twice as stiff, while the two tofu products range from $E = 22.3\,\text{kPa}$ to $E = 34.0\,\text{kPa}$ and are about half as stiff. Our discovered stiffness values lie well within the range of the reported compression stiffnesses for sausage of $E = 120\,\text{kPa}$, turkey of $E = 90\,\text{kPa}$, and chicken of $E = 40\,\text{kPa}$ [24] using traditional texture profiling analysis [23]; the reported tensile stiffnesses for chicken of $E = 360\,\text{kPa}$ and soy protein of $E = 100\,\text{kPa}$ using tensile testing [25]; and our previous study of tofurky of $E = 282\,\text{kPa}$, plant-based chicken of $E = 108\,\text{kPa}$, and real chicken of $E = 87\,\text{kPa}$ using tension, compression, and shear testing [27]. Our results suggests that, when looking for vegetarian options, we no longer have to rely on tofu alone. Tofu, a protein- and vitamin-rich product of curdled soy milk, was first produced nearly 2,000 years ago in China, and has since then become a popular substitute for meat worldwide [34]. Today, tofu comes in various stiffnesses: soft, silken, regular, firm, and extra firm. Its stiffness is tunable by its water content that ranges from 85-90% for soft to 40%-50% for extra firm. In our study, even firm and extra firm tofu consistently display the lowest stiffness

across all products and tests, and perform poorly in reproducing the mechanical properties of animal meat. In contrast, plant-based sausage and hotdog successfully mimic the mechanical signature of their animal-based counterparts. Interestingly, market analyses predict that of the different plant-based meat products, burgers, patties, ground, nuggets, and sausages, the sausage market will experience the highest growth rate within the next decade [35]. As one of the most common protein-based breakfast foods, plant-based sausage comes in a variety of flavors and is in high demand worldwide. Yet, as we can see in Table 1, the growing success of plant-based sausage and hotdog comes at a price: a high sodium content, added sugars, and long list of highly processed ingredients [36].

The more processed the product, the more complex the mechanics. In this study, we perform the first fully three-dimensional characterization of eight different artificial and real meat products. We analyze the data using a constitutive neural network with L_0-regularization [28] to discover the best one- and two-term models that simultaneously fit the tension, compression, and shear data for each product. Using the error plots in Figure 3 and the discovered weights in Table 1, we can easily write out the free energy functions that best fit each meat. Strikingly, the oldest and simplest of all models, the classical widely used neo Hooke model [31] in terms of only I_1 is the best model for firm and extra firm tofu, the two softest, oldest, and simplest products with the shortest list of ingredients: water, soybeans, calcium sulfate, and calcium or magnesium chloride. The popular Mooney Rivlin model [32, 33] in terms of I_1 and I_2 is the best model for tofurky and plant sausage, the two stiffest products. Interestingly, we discover three novel, nonlinear material models for the three highly processed real meats: real sausage in terms of I_1 and $\exp(I_1^2)$, real hotdog in terms of I_1 and I_2^2, and spam turkey in terms of I_1 and I_1^2. This suggests that processed real meat has a complex mechanical behavior that is not appropriately acknowledged by common existing constitutive models. Surprisingly, the degree of complexity of our discovered material models, from one-term to two-term and from linear to quadratic or exponential, mimics the complexity of the ingredient list, from a few pure ingredients for tofu to numerous highly processed ingredients for sausage and hotdog. Discovering product-specific best-fit models from data would have been unthinkable one or two decades ago, and is only now made possible by recent developments in constitutive neural networks, machine learning, and artificial intelligence [28]. This suggests that, instead of using a trial-and-error approach to improve the texture of plant-based meat, we could envision using generative artificial intelligence to scientifically generate recipes for plant-based meat products with precisely desired properties.

Animal-based products are stiffer in tension than in compression, while plant-based products are not. An insightful mechanical property that is impossible to quantify by a double-compression texture profiling analysis alone [23] is tension-compression asymmetry. Our combined tension, compression, and shear tests in Figures 1 and 2 **k** reveal that the three animal-based meats display the highest tension-compression asymmetry, with 2.41 for real sausage, 1.41 for real hotdog, and 1.39 for spam turkey. Interestingly, all plant-based products, except for extra firm tofu, are either close to symmetric or stiffer in compression than in tension with values smaller than one, with 1.03 for plant hotdog, 0.95 for firm tofu, 0.79 for plant sausage, and 0.70 for tofurky. Similarly, all three animal-based meats rank amongst the four products with the highest failure stress of 26.0 kPa for real hotdog, 21.4 kPa for real sausage, and 16.3 kPa for spam turkey, in 2 **i**, while all plant-based products, except for tofurky, have significantly lower failure stresses. Understanding the mechanical properties of plant-based protein is a rapidly growing field of research [25]. Naturally, the tensile, compressive, and shear stiffnesses in Figure 2 are highly sensitive to plant source and processing [34], and successful formulations often benefit from protein synergies, such as soy and wheat or pea and potato [14]. In addition, the complex ingredient lists in Table 1 suggest that tunability may require other non-protein components such as oil or starch. Instead of applying our technology only to a *forward analysis*, where we test an existing product and characterize its mechanical features, can we perform an *inverse analysis*, where we prescribe desired mechanical features and determine the required ingredient list? Our study demonstrates that constitutive neural networks provide a powerful tool to learn functional mappings between products and texture [27]. What if we could expand this technology to learn inverse mappings between texture and ingredients to fine-tune the mechanical signature of plant-based meat?

In summary, our results confirm that in seeking to design plant-based alternatives that truly mimic the sensory experience of animal meat, it is not enough to rely on traditional one-dimensional double compression tests. Instead, we need to consider fully three-dimensional testing to discover the true material behavior across a broad loading range, and understand the subtle mechanical differences that may trigger differences in our perception of taste.

Our study shows that the one-dimensional stiffness of artificial and real sausage and hotdog is nearly identical, but their three-dimensional characteristics are not. Our approach to automatically discover the mechanics of real and artificial meat with constitutive neural networks could be a starting point towards using generative artificial intelligence to reverse-engineer formulas for plant-based meat products with customer-friendly tunable properties. We envision that the present work encourages others, especially in academia or nonprofit organizations who can freely share their results, to undertake similar but complementary studies and create an open source data base of the mechanical signatures of real and artificial meat to accelerate discovery and innovation towards a more efficient and sustainable global food system.

Methods

Mechanical testing. We tested five plant-based meat products: ham style roast tofurky (Tofurky, Hood River, OR), artesian vegan frankfurter plant sausage (Field Roast, Seattle, WA), signature stadium plant hotdog (Field Roast, Seattle, WA), organic firm tofu (365 by Whole Foods Market, Austin TX), organic extra firm tofu (House Foods, Garden Grove, CA). For comparison, we also tested three animal-based meat products: wieners classic real hotdog (Oscar Meyer, Kraft Heinz Co, Chicago, IL), oven roasted spam turkey (Spam, Hormel Foods Co, Austin, MN), and turkey polska kielbasa real sausage (Hillshire Farm, New London, WI). Table 1 summarizes the ingredients of all eight products. For each meat type, we tested at least $n = 5$ samples in tension, compression, and shear. Figure 4 documents our sample preparation and our mechanical testing.

Sample preparation. We prepare the samples following our established protocols [27]. Figures 4 **b,c,e,f** illustrate our tension tests, for which we use a custom 3D printed cutting guide and brain sectioning knife to prepare samples of $1\times1\times2\,\text{cm}^3$. We super glue the samples to glass microscope slides and wait for 30 minutes until the glue is fully cured. During curing, we drape a damp paper towel over the samples to keep them hydrated. For the compression and shear tests, we prepare cylindrical samples of 8 mm diameter and 1 cm height using a biopsy punch to extract full-thickness cores from the center of each material, and store the samples in a damp paper tower until testing.

Sample testing. For all three modes, tension, compression, and shear, we test the samples raw and at room temperature at 25°C [27]. We perform all uniaxial tension tests using an Instron 5848 (Instron, Canton, MA) with a 100N load cell, see Figure 4 **e**. We use 3D printed custom grips to rapidly mount and unmount the microscope slides for high throughput testing. Figure 5 in the Extended Data shows the part dimensions to create these grips. We mount each sample in the grips, apply a small pre-load, and calibrate the initial gauge length L. We determine the pre-load magnitude for each sample individually. We define pre-load as the minimum load needed to remove any slack, based on visual inspection of a force-displacement curve starting with a fully unloaded specimen, generally on the order of 0.5 N. We then increase the tensile stretch quasi-statically at a rate of $\dot{\lambda} = 0.2\%/\text{s}$ for $t = 50$ s, until the sample fails. We perform all uniaxial compression and shear tests using an AR-2000ex torsional rheometer (TA Instruments, New Castle, DE), see Figure 4 **d**. For the compression tests, we mount the sample, apply a small pre-load, and calibrate the initial gage length L. We determine the pre-load for each sample based on its loading curve, with values on the order of 0.5 N. We then increase the compressive stretch quasi-statically at a rate of $\dot{\lambda} = 0.2\%/\text{s}$ for $t = 50$ s, up to a total stretch of $\lambda = 0.9$. For the shear tests, we apply a 10% compressive pre-load and calibrate the initial gage length L. We then rotate the upper plate quasi-statically at a shear rate of $\dot{\gamma} = 0.2\%/\text{s}$ for $t = 50$ s, up to a total shear of $\gamma = 0.1$. To prevent slippage of the samples during the shear tests, we use a sandpaper-covered base plate of 20 mm diameter and a sandpaper-covered top plate of 8 mm diameter.

Analytical methods and data processing. For each sample and each test mode, we use MATLAB (Mathworks, Natick, MA, USA) to smooth the curves using `smoothingspline` and `SmoothingParam = 1`. We interpolate each smooth curve over 21 equidistant points in the ranges $1.0 \leq \lambda \leq \lambda_{\max}$ for tension, $1.0 \geq \lambda \geq 0.9$ for compression, and $0.0 \leq \gamma \leq 1.0$ for shear. For each meat product, we select $\lambda_{\max}$ in tension as the maximum stretch in the hyperelastic regime, the loading range within which we observe no visible failure for any of the samples. Finally, we average the interpolated curves to obtain the mean and standard error of the mean for each product and report the data in Table 2 of the Extended Data.

Stiffness. For each testing mode, we extract the stiffness of each product from the data in Table 2 using linear regression. We convert that the tension and compression data $\{\lambda; P_{11}\}$ into strain-stress pairs $\{\varepsilon; \sigma\}$, where $\varepsilon = \lambda - 1$ is the strain and

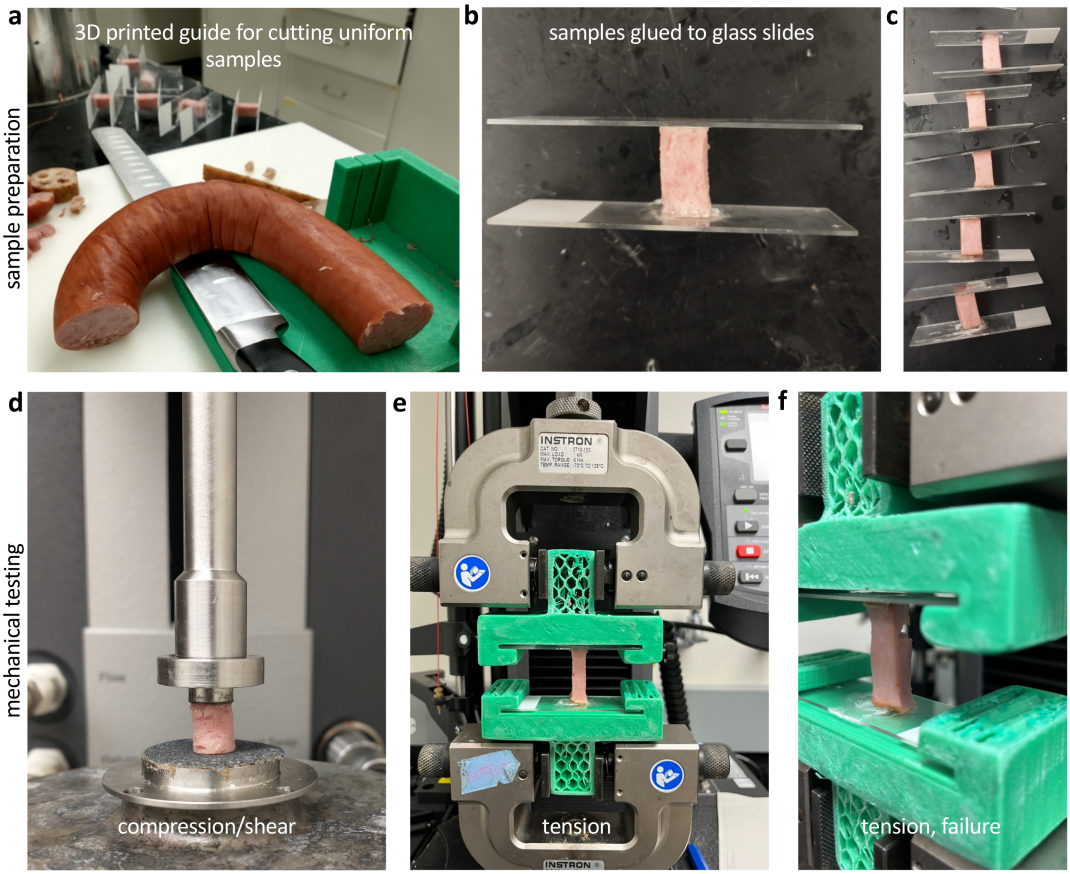

Fig. 4 Sample preparation and mechanical testing. a. Samples are cut using a 3D printed guide and a brain sectioning knife to obtain uniform dimensions of $1{\times}1{\times}2\,\mathrm{cm}^3$ for tensile testing. **b.** Samples are super glued to glass microscope slides. **c.** Samples are left to set for 30-45 minutes for the glue to adhere. **d.** Cylindrical samples of 8 mm diameter and 1 cm height are cored using a biopsy punch and loaded into a rheometer for compression and shear testing using parallel plates with sandpaper on both surfaces. **e.** Tension samples are loaded into 3D printed grips, which are compatible with an Instron testing device. **f.** Tension test is run until the sample fails. **a, b, d** show real sausage and **c, e, f** show real hotdog.

$\sigma = P_{11}$ is the stress. We postulate a linear stress-strain relation, $\sigma = E \cdot \varepsilon$, and use linear regression to determine the tensile and compressive stiffnesses $E_{\mathrm{ten}}, E_{\mathrm{com}} = (\boldsymbol{\varepsilon} \cdot \hat{\boldsymbol{\sigma}})/(\boldsymbol{\varepsilon} \cdot \boldsymbol{\varepsilon})$. Similarly, we rewrite the shear data, $\{\gamma; P_{12}\}$, as shear strain-stress pairs $\{\gamma; \tau\}$, where γ is the shear strain and $\tau = P_{12}$ is the shear stress. We postulate a linear shear stress-strain relation, $\tau = \mu \cdot \gamma$, convert the shear modulus μ into the shear stiffness, $E_{\mathrm{shr}} = 2\,[\,1 + \nu\,]\,\mu = 3\,\mu$, and use linear regression, to determine the shear stiffness $E_{\mathrm{shr}} = 3\,(\boldsymbol{\gamma} \cdot \hat{\boldsymbol{\tau}})/(\boldsymbol{\gamma} \cdot \boldsymbol{\gamma})$.

Kinematics. We analyze all three testing modes combined using finite deformation continuum mechanics [37, 38]. During testing, particles $\boldsymbol{X}$ of the undeformed sample map to particles, $\boldsymbol{x} = \boldsymbol{\varphi}(\boldsymbol{X})$, of the deformed sample via the deformation map $\boldsymbol{\varphi}$. Similarly, line elements of the $\mathrm{d}\boldsymbol{X}$ of the undeformed sample map to line elements, $\mathrm{d}\boldsymbol{x} = \boldsymbol{F} \cdot \mathrm{d}\boldsymbol{X}$, of the deformed sample via the deformation gradient, $\boldsymbol{F} = \nabla_{\boldsymbol{X}} \boldsymbol{\varphi} = \sum_{i=1}^{3} \lambda_i\, \boldsymbol{n}_i \otimes \boldsymbol{N}_i$. Its spectral representation introduces the principal stretches λ_i and the principal directions $\boldsymbol{N}_i$ and $\boldsymbol{n}_i$ in the undeformed and deformed configurations, where $\boldsymbol{F} \cdot \boldsymbol{N}_i = \lambda_i \boldsymbol{n}_i$. We assume that all meat samples are isotropic and have three principal invariants, $I_1 = \lambda_1^2 + \lambda_2^2 + \lambda_3^2$ and $I_2 = \lambda_1^2\lambda_2^2 + \lambda_2^2\lambda_3^2 + \lambda_1^2\lambda_3^2$ and $I_3 = \lambda_1^2\,\lambda_2^2\,\lambda_3^2 = J^2$, which are linear, quadratic, and cubic in terms of the principal stretches squared. We also assume that all samples are perfectly incompressible, and their third invariant always remains equal to one, $I_3 = 1$. The remaining two invariants, I_1 and I_2, depend on the type of experiment.

Constitutive equations. Constitutive equations relate a stress like the Piola or nominal stress $\boldsymbol{P}$, the force per undeformed area that we measure during our experiments, to a deformation measure like the deformation gradient $\boldsymbol{F}$ [27]. For a hyperelastic material that satisfies the second law of thermodynamics, we can express the Piola stress, $\boldsymbol{P} = \partial\psi(\boldsymbol{F})/\partial\boldsymbol{F} - p\,\boldsymbol{F}^{-\mathrm{t}}$, as the derivative of the

Helmholtz free energy function $\psi(\boldsymbol{F})$ with respect to the deformation gradient $\boldsymbol{F}$, modified by a pressure term, $-p\,\boldsymbol{F}^{-\mathrm{t}}$, to ensure perfect incompressibility. Here, the hydrostatic pressure, $p = -\frac{1}{3}\,\boldsymbol{P} : \boldsymbol{F}$, acts as a Lagrange multiplier that that we determine from the boundary conditions of our experiments. Instead of formulating the free energy function directly in terms of the deformation gradient $\psi(\boldsymbol{F})$, we can express it in terms of the invariants, $\psi(I_1, I_2)$, and obtain the following expression, $\boldsymbol{P} = \partial\psi/\partial I_1 \cdot \partial I_1/\partial\boldsymbol{F} + \partial\psi/\partial I_2 \cdot \partial I_2/\partial\boldsymbol{F} - p\,\boldsymbol{F}^{-\mathrm{t}}$.

Constitutive neural networks. Motivated by these kinematic and constitutive considerations, we reverse-engineer our own constitutive neural network that satisfies the conditions of thermodynamic consistency, material objectivity, material symmetry, incompressibility, constitutive restrictions, and polyconvexity by design [28, 39]. Yet, instead of building these constraints into the loss function, we hardwire them directly into our network input, output, architecture, and activation functions [40, 41] to satisfy the fundamental laws of physics. Special members of this family represent well-known constitutive models, including the neo Hooke [31], Blatz Ko [29], Mooney Rivlin [32, 33], and Demiray [30] models, for which the network weights gain a clear physical interpretation [39, 42]. Specifically, our constitutive neural network learns a free energy function that is parameterized in terms of the first and second invariants. It takes the deformation gradient $\boldsymbol{F}$ as input, computes the two invariants, I_1 and I_2, raises them to the first and second powers, $(\circ)$ and $(\circ)^2$, applies either the identity or exponential function, $(\circ)$ and $\exp(\circ)$, and summarizes all eight terms in the strain energy function ψ as the network output. Figure 6 illustrates our network with $n = 8$ nodes, with the following eight-term free energy function,

$$\begin{aligned}\psi(I_1, I_2) = {} & w_1\,[I_1 - 3] + w_2\,[\exp(w_2^*[I_1 - 3]) - 1] \\ & + w_3\,[I_1 - 3]^2 + w_4\,[\exp(w_4^*[I_1 - 3]^2) - 1] \\ & + w_5\,[I_2 - 3] + w_6\,[\exp(w_6^*[I_2 - 3]) - 1] \\ & + w_7\,[I_2 - 3]^2 + w_8\,[\exp(w_8^*[I_2 - 3]^2) - 1]\,,\end{aligned}$$

where $\boldsymbol{w} = [\,w_1, w_2, w_3, w_4, w_5, w_6, w_7, w_8\,]$ and $\boldsymbol{w}^* = [\,w_2^*, w_4^*, w_6^*, w_8^*]$ are the network weights. From the derivative of the free energy, we calculate the stress,

$$\begin{aligned}\boldsymbol{P} = {} & [w_1 + w_2 \exp(w_2^*[I_1 - 3]) \\ & + 2\,[I_1 - 3]\,[w_3 + w_4 \exp(w_4^*[I_1 - 3]^2)]]\partial I_1/\partial\boldsymbol{F} \\ & + [w_5 + w_6 \exp(w_6^*[I_2 - 3]) \\ & + 2\,[I_2 - 3]\,[w_7 + w_8 \exp(w_8^*[I_2 - 3]^2)]]\partial I_2/\partial\boldsymbol{F},\end{aligned}$$

where the derivatives of the invariants, $\partial I_1/\partial\boldsymbol{F}$ and $\partial I_2/\partial\boldsymbol{F}$, depend on the type or experiment. During training, our network autonomously discovers the best subset of activation functions from $2^8 - 1 = 255$ possible combinations of terms. At the same time, it naturally trains the weights of the less important terms to zero.

Uniaxial tension and compression. In the tension and compression experiments, we apply a stretch $\lambda = l/L$, that we calculate as the ratio between the current and initial sample lengths l and L. We can write the deformation gradient $\boldsymbol{F}$ in matrix representation as

$$\boldsymbol{F} = \begin{bmatrix} \lambda & 0 & 0 \\ 0 & 1/\sqrt{\lambda} & 0 \\ 0 & 0 & 1/\sqrt{\lambda} \end{bmatrix} \quad \text{with} \quad \lambda = l/L\,.$$

In tension and compression, the first and second invariants and their derivatives are $I_1 = \lambda^2 + 2/\lambda$ and $I_2 = 2\lambda + 1/\lambda^2$ with $\partial_\lambda I_1 = 2\,\lambda - 2/\lambda^2$ and $\partial_\lambda I_2 = 2 - 2/\lambda^3$. Using the zero normal stress condition, $P_{22} = P_{33} = 0$, we obtain the explicit expression for the uniaxial stress, $P_{11} = 2\,[\lambda - 1/\lambda^2]\,\partial\psi/\partial I_1 + 2\,[1 - 1/\lambda^3]\,\partial\psi/\partial I_2$, which we can write explicitly in terms of the network weights $\boldsymbol{w}$ and $\boldsymbol{w}^*$,

$$\begin{aligned}P_{11} = {} & 2\,\left[\lambda - 1/\lambda^2\right]\,[\,w_1 + w_2 \exp(w_2^*[I_1 - 3]) \\ & + 2\,[I_1 - 3]\,[\,w_3 + w_4 \exp(w_4^*[I_1 - 3]^2)]] \\ & + 2\,\left[1 - 1/\lambda^3\right]\,[\,w_5 + w_6 \exp(w_6^*[I_2 - 3]) \\ & + 2\,[I_2 - 3]\,[\,w_7 + w_8 \exp(w_8^*[I_2 - 3]^2)]].\end{aligned}$$

Simple shear. In the shear experiment, we apply a torsion angle ϕ, that translates into the shear stress, $\gamma = r/L\,\phi$, by multiplying it with the sample radius r and dividing by the initial sample length L. We can write the deformation gradient $\boldsymbol{F}$ in matrix representation as

$$\boldsymbol{F} = \begin{bmatrix} 1 & \gamma & 0 \\ 0 & 1 & 0 \\ 0 & 0 & 1 \end{bmatrix} \quad \text{with} \quad \gamma = r/L\,\phi\,.$$

In shear, the first and second invariants and their derivatives are $I_1 = 3 + \gamma^2$ and $I_2 = 3 + \gamma^2$ with $\partial_\gamma I_1 = 2\,\gamma$ and $\partial_\gamma I_2 = 2\,\gamma$. We obtain the explicit expression for the shear stress, $P_{12} = 2\,[\partial\psi/\partial I_1 + \partial\psi/\partial I_2]\,\gamma$, which we can write explicitly in terms of the network weights $\boldsymbol{w}$ and $\boldsymbol{w}^*$,

$$\begin{aligned}P_{12} = {} & 2\,\gamma\,[\,w_1 + w_2 \exp(w_2^*[I_1 - 3]) \\ & + 2\,[I_1 - 3]\,[\,w_3 + w_4 \exp(w_4^*[I_1 - 3]^2)]] \\ & + 2\,\gamma\,[\,w_5 + w_6 \exp(w_6^*[I_2 - 3]) \\ & + 2\,[I_2 - 3]\,[\,w_7 + w_8 \exp(w_8^*[I_2 - 3]^2)]].\end{aligned}$$

Loss function. Our constitutive neural network learns the network weights, $\boldsymbol{w}$ and $\boldsymbol{w}^*$, by minimizing the loss function L that penalizes the mean squared error, the L_2-norm of the difference between model and data, divided by the number of data points in tension, compression, and shear [27],

$$\begin{aligned} L = & \frac{1}{n_{\text{ten}}} \sum_{i=1}^{n_{\text{ten}}} ||P_{\text{ten}}(\lambda_i) - \hat{P}_{\text{ten,i}}||^2 \\ & + \frac{1}{n_{\text{com}}} \sum_{i=1}^{n_{\text{com}}} ||P_{\text{com}}(\lambda_i) - \hat{P}_{\text{com,i}}||^2 \\ & + \frac{1}{n_{\text{shr}}} \sum_{i=1}^{n_{\text{shr}}} ||P_{\text{shr}}(\gamma_i) - \hat{P}_{\text{shr,i}}||^2 \rightarrow \min \end{aligned}$$

We train the network by minimizing the loss function with the ADAM optimizer, a robust adaptive algorithm for gradient-based first-order optimization using the tension, compression, and shear data for all eight meat products from Table 2.

Best-in-class modeling. Instead of looking for the best possible fit of the models to the experimental data, we seek to discover meaningful constitutive models that are *interpretable* and *generalizable* [43], models that have a sparse parameter vector with a limited number of terms [44]. From combinatorics, we know that our network can discover $2^8 - 1 = 255$ possible models, 8 with a single term, 28 with two, 56 with three, 70 with four, 56 with five, 28 with six, 8 with seven, and 1 with all eight terms. For practical purposes, we focus on the the 8 one-term models and the 28 two-term models, set all other weights to zero, and discover the non-zero weights that characterize the active terms. We summarize the results in a color-coded 8×8 error plot, as the average of the mean squared error across the tension, compression, and shear data, and report the parameters of the best-in-class one- and two-term models in Table 1.

Acknowledgments This project was supported by the NSF Graduate Research Fellowship to SSP, by the Emmy Noether Grant 533187597 to Kevin Linka, and by the NSF CMMI Award 2320933 and the ERC Advanced Grant 101141626 to EK.

Conflicts of interest All authors declare no financial competing interests.

Availability of data and materials The data are available in Table 2 as well as at https://github.com/LivingMatterLab/CANN.

Code availability The constitutive network code is available at https://github.com/LivingMatterLab/CANN.

Authors' contributions SS designed the 3D printed grips, contributed to the code, conducted the analyses, and wrote the paper. SS and ED designed and oversaw the testing protocols. DA, MA, AD, RD, YL, MPV, and VPM performed the experimental testing. KL wrote the constitutive neural network code. ML and EK conceptualized the project and edited the paper.

References

[1] Friedrich, B. Transforming a 12,000-year-old technology. *Nature Food* **3**, 807–808 (2022).

[2] Humpenöder, F. *et al.* Projected environmental benefits of replacing beef with microbial protein. *Nature* **605**, 90–96 (2022).

[3] Searchinger, T. *et al.* Creating a sustainable food future: A menu of solutions to sustainably feed more than 9 billion people by 2050. *World Resources Institute, Washington DC* (2019).

[4] Wirsenius, S., Azar, C. & Berndes, G. How much land is needed for global food production under scenarios of dietary changes and livestock productivity increases in 2030? *Agricultural Systems* **103**, 621–638 (2010).

[5] Hong, C. *et al.* Global and regional drivers of land-use emissions in 1961–2017. *Nature* **589**, 554–561 (2021).

[6] Eisen, M. B. & Brown, P. O. Rapid global phaseout of animal agriculture has the potential to stabilize greenhouse gas levels for 30 years and offset 68 percent of co_2 emissions this century. *PLOS Climate* **1**, e0000010 (2022).

[7] Poore, J. & Nemecek, T. Reducing food's environmental impacts through producers and consumers. *Science* **360**, 987–992 (2018).

[8] Gerber, P. J. *et al.* Tackling climate change through livestock. A global assessment of emissions and mitigation opportunities. *Food and Agriculture Organization of the United Nations, Rome* (2013).

[9] Clark, M. A. *et al.* Global food system emissions could preclude achieving the 1.5° and 2°C climate change targets. *Science* **370**, 705–708 (2020).

[10] McNamara, E. & Bornkamp, C. Cultivated meat as a tool for fighting antimicrobial resistance. *Nature Food* **3**, 791–794 (2022).

[11] Van Boeckel, T. P. *et al.* Global trends in antimicrobial use in food animals. *Proceedings of the National Academy of Sciences* **112**, 5649–5654 (2015).

[12] Willyard, C. Drug-restistant bacteria ranked. *Nature* **543**, 15 (2017).

[13] González, N., Marquès, M., Nadal, M. & Domingo, J. L. Meat consumption: Which are the current global risks? A review of recent (2010–2020) evidences. *Food Research International* **137**, 109341 (2020).

[14] Good Food Institute. Plant protein primer. https://gfi.org/resource/plant-protein-primer (2024).

[15] Smetana, S. *et al.* Meat substitutes: Resource demands and environmental footprints. *Resources, Conservation, and Recycling* **190**, 106831 (2023).

[16] Szenderák, J., Fróna, D. & Rákos, M. Consumer acceptance of plant-based meat substitutes: A narrative review. *Foods* **11**, 1274 (2022).

[17] Dagevos, H. Finding flexitarians: Current studies on meat eaters and meat reducers. *Trends in Food Science & Technology* **114**, 530–539 (2021).

[18] Bryant, C., Szejda, K., Parekh, N., Deshpande, V. & Tse, B. A survey of consumer perceptions of plant-based and clean meat in the USA, India, and China. *Frontiers in Sustainable Food Systems* **3** (2019).

[19] Clifford Astbury, C. Health and sustainability of everyday food. *Nature Food* **4**, 357 (2023).

[20] Szczesniak, A. S. Texture is a sensory property. *Food Quality and Preference* **13**, 215–225 (2002).

[21] Nishinari, K. & Fang, Y. Perception and measurement of food texture: Solid foods. *Journal of Texture Studies* **49**, 160–201 (2018).

[22] Bourne, M. C. *Food Texture and Viscosity: Concept and Measurement* 2nd edn (Academic Press, San Diego., 2002).

[23] Friedman, H. H., Whitney, J. E. & Szczesniak, A. S. The texturometer–A new instrument for objective texture measurement. *Journal of Food Science* **28**, 390–396 (1963).

[24] Paredes, J., Cortizo-Lacalle, D., Imaz, A. M., Aldazabel, J. & Vila, M. Application of texture analysis methods for the characterization of cultured meat. *Scientific Reports* **12**, 3898 (2022).

[25] Ko, C., Davies, A. & Auty, M. Putting meat to the test: Imaging and mechanical testing used to understand the properties of meat alternatives and how they mimic our typical meat sensory experience. *Microscopy Today* **31**, 21–25 (2023).

[26] Lepetit, J. & Culioli, J. Mechanical properties of meat. *Meat Science* **36**, 203–237 (1994).

[27] St. Pierre, S. R. *et al.* Discovering the mechanics of artificial and real meat. *Computer Methods in Applied Mechanics and Engineering* **415**, 116236 (2023).

[28] Linka, K. & Kuhl, E. A new family of constitutive artificial neural networks towards automated model discovery. *Computer Methods in Applied Mechanics and Engineering* **403**, 115731 (2023).

[29] Blatz, P. J. & Ko, W. L. Application of finite elastic theory to the deformation of rubbery materials. *Transactions of the Society of Rheology* **6**, 223–252 (1962).

[30] Demiray, H. A note on the elasticity of soft biological tissues. *Journal of Biomechanics* **5**, 309–311 (1972).

[31] Treloar, L. Stresses and birefringence in rubber subjected to general homogeneous strain. *Proceedings of the Physical Society* **60**, 135 (1948).

[32] Mooney, M. A theory of large elastic deformation. *Journal of Applied Physics* **11**, 582–592 (1940).

[33] Rivlin, R. S. Large elastic deformations of isotropic materials iv. further developments of the general theory. *Philosophical Transactions of the Royal Society London A* **241**, 379–397 (1948).

[34] Guan, X. *et al.* Changes of soybean protein during tofu processing. *Foods* **10**, 1594 (2021).

[35] *Plant-based meat market* (Straits Research, Maharashtra India, 2023).

[36] Curtain, F. & Grafenauer, S. Plant-based meat substitutes in the flexitarian age: An audit of products on supermarket shelves. *Nutrients* **11**, 2603 (2019).

[37] Antman, S. S. *Nonlinear Problems of Elasticity* (Springer-Verlag, New York., 2005).

[38] Holzapfel, G. A. *Nonlinear Solid Mechanics: A Continuum Approach to Engineering* (John Wiley & Sons, Chichester, 2000).

[39] Linka, K., St. Pierre, S. R. & Kuhl, E. Automated model discovery for human brain using constitutive artificial neural networks. *Acta Biomaterialia* **160**, 134–1510 (2023).

[40] Holzapfel, G. A., Linka, K., Sherifova, S. & Cyron, C. Predictive constitutive modelling of arteries by deep learning. *Journal of the Royal Society Interface* **18**, 20210411 (2021).

[41] Tac, V., Sahli Costabal, F. & Buganza Tepole, A. Data-driven tissue mechanics with polyconvex neural ordinary differential equations. *Computer Methods in Applied Mechanics and Engineering* **398**, 115248 (2022).

[42] St. Pierre, S. R., Linka, K. & Kuhl, E. Principal-stretch-based constitutive neural networks autonomously discover a subclass of ogden models for human brain tissue. *Brain Multiphysics* **4**, 100066 (2023).

[43] Brunton, S. L., Proctor, J. P. & Kutz, J. N. Discovering governing equations from data by sparse identification of nonlinear dynamical systems. *Proceedings of the National Academy of Sciences* **113**, 3932–3937 (2016).

[44] McCulloch, J. A., St. Pierre, S. R., Linka, K. & Kuhl, E. On sparse regression, Lp-regularization, and automated model discovery (2024).

Extended data

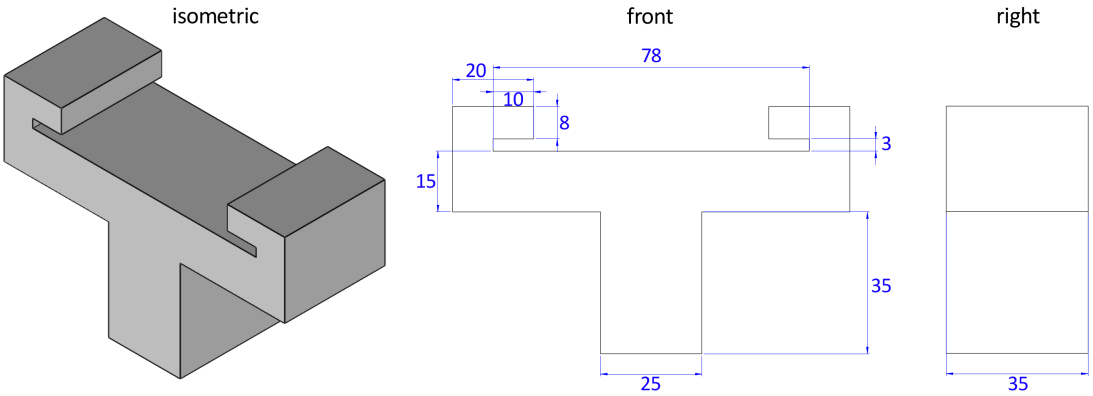

Fig. 5 Design of mechanical device for tensile testing. Front, right, and isometric views of our customized 3D printed device to hold glass slides during tensile testing. Two holders need to be printed to complete the set-up. A standard microscope glass slide fits into the 3 mm slot; it mounts and unmounts easily for high throughout testing. All dimensions are in mm.

Table 2 Real and plant-based meats tested in tension, compression, and shear. Stresses are reported as means from the loading and unloading curves of n samples tested in the ranges $1.0 \leq \lambda \leq \lambda_{\max}$ for tension, $1.0 \geq \lambda \geq 0.9$ for compression $0.0 \leq \gamma \leq 0.1$ for shear. The maximum tensile stretch $\lambda_{\max}$ is product dependent and denotes the stretch before failure occurs, so before the stress-stretch curve displays a significant drop.

tofurky						plant sausage						spam turkey					
tension $n=5$		compression $n=8$		shear $n=8$		tension $n=5$		compression $n=8$		shear $n=8$		tension $n=5$		compression $n=8$		shear $n=8$	
λ [-]	P_{11} [kPa]	λ [-]	P_{11} [kPa]	γ [-]	P_{12} [kPa]	λ [-]	P_{11} [kPa]	λ [-]	P_{11} [kPa]	γ [-]	P_{12} [kPa]	λ [-]	P_{11} [kPa]	λ [-]	P_{11} [kPa]	γ [-]	P_{12} [kPa]
1.000	0.000	1.000	0.000	0.000	0.000	1.000	0.000	1.000	0.000	0.000	0.000	1.000	0.000	1.000	0.000	0.000	0.000
1.005	1.320	0.995	-1.512	0.005	0.596	1.008	1.513	0.995	-0.744	0.005	0.250	1.008	1.243	0.995	-0.461	0.005	0.176
1.010	2.532	0.990	-2.633	0.010	1.079	1.015	2.648	0.990	-1.370	0.010	0.473	1.015	2.247	0.990	-0.764	0.010	0.325
1.015	3.599	0.985	-3.765	0.015	1.519	1.023	3.465	0.985	-1.943	0.015	0.670	1.023	3.152	0.985	-1.148	0.015	0.463
1.020	4.550	0.980	-4.836	0.020	1.930	1.030	4.105	0.980	-2.448	0.020	0.851	1.030	3.988	0.980	-1.466	0.020	0.592
1.025	5.429	0.975	-5.885	0.025	2.302	1.038	4.653	0.975	-3.003	0.025	1.033	1.038	4.759	0.975	-1.816	0.025	0.714
1.030	6.257	0.970	-6.981	0.030	2.680	1.045	5.164	0.970	-3.481	0.030	1.204	1.045	5.501	0.970	-2.173	0.030	0.831
1.035	7.048	0.965	-8.031	0.035	3.037	1.053	5.613	0.965	-3.959	0.035	1.367	1.053	6.205	0.965	-2.491	0.035	0.949
1.040	7.787	0.960	-9.023	0.040	3.388	1.060	6.053	0.960	-4.488	0.040	1.526	1.060	6.897	0.960	-2.866	0.040	1.059
1.045	8.505	0.955	-10.227	0.045	3.740	1.068	6.479	0.955	-5.000	0.045	1.681	1.068	7.577	0.955	-3.118	0.045	1.165
1.050	9.222	0.950	-11.214	0.050	4.068	1.075	6.893	0.950	-5.454	0.050	1.831	1.075	8.236	0.950	-3.550	0.050	1.267
1.055	9.910	0.945	-12.339	0.055	4.387	1.083	7.278	0.945	-5.991	0.055	1.977	1.083	8.870	0.945	-3.853	0.055	1.371
1.060	10.585	0.940	-13.382	0.060	4.698	1.090	7.675	0.940	-6.386	0.060	2.119	1.090	9.489	0.940	-4.267	0.060	1.469
1.065	11.256	0.935	-14.478	0.065	5.002	1.098	8.064	0.935	-6.945	0.065	2.258	1.098	10.101	0.935	-4.618	0.065	1.565
1.070	11.904	0.930	-15.581	0.070	5.296	1.105	8.450	0.930	-7.347	0.070	2.394	1.105	10.688	0.930	-4.983	0.070	1.657
1.075	12.529	0.925	-16.627	0.075	5.595	1.113	8.810	0.925	-7.947	0.075	2.528	1.113	11.233	0.925	-5.367	0.075	1.748
1.080	13.149	0.920	-17.801	0.080	5.877	1.120	9.168	0.920	-8.405	0.080	2.659	1.120	11.794	0.920	-5.807	0.080	1.834
1.085	13.757	0.915	-18.819	0.085	6.149	1.128	9.517	0.915	-8.872	0.085	2.786	1.128	12.326	0.915	-6.118	0.085	1.919
1.090	14.329	0.910	-19.956	0.090	6.431	1.135	9.862	0.910	-9.470	0.090	2.912	1.135	12.861	0.910	-6.573	0.090	2.001
1.095	14.875	0.905	-20.970	0.095	6.703	1.143	10.194	0.905	-9.909	0.095	3.034	1.143	13.376	0.905	-6.932	0.095	2.078
1.100	15.366	0.900	-22.081	0.100	6.966	1.150	10.479	0.900	-10.433	0.100	3.156	1.150	13.836	0.900	-7.389	0.100	2.152

real sausage						real hotdog						plant hotdog					
tension $n=6$		compression $n=7$		shear $n=7$		tension $n=8$		compression $n=7$		shear $n=7$		tension $n=6$		compression $n=6$		shear $n=6$	
λ [-]	P_{11} [kPa]	λ [-]	P_{11} [kPa]	γ [-]	P_{12} [kPa]	λ [-]	P_{11} [kPa]	λ [-]	P_{11} [kPa]	γ [-]	P_{12} [kPa]	λ [-]	P_{11} [kPa]	λ [-]	P_{11} [kPa]	γ [-]	P_{12} [kPa]
1.000	0.000	1.000	0.000	0.000	0.000	1.000	0.000	1.000	0.000	0.000	0.000	1.000	0.000	1.000	0.000	0.000	0.000
1.008	0.980	0.995	-0.216	0.005	0.075	1.018	1.374	0.995	-0.271	0.005	0.085	1.010	0.679	0.995	-0.256	0.005	0.094
1.015	1.838	0.990	-0.459	0.010	0.138	1.035	2.352	0.990	-0.456	0.010	0.158	1.020	1.162	0.990	-0.567	0.010	0.166
1.023	2.659	0.985	-0.618	0.015	0.197	1.053	3.289	0.985	-0.724	0.015	0.221	1.030	1.591	0.985	-0.739	0.015	0.240
1.030	3.452	0.980	-0.827	0.020	0.251	1.070	4.202	0.980	-0.910	0.020	0.282	1.040	2.030	0.980	-0.997	0.020	0.306
1.038	4.252	0.975	-1.015	0.025	0.300	1.088	5.156	0.975	-1.055	0.025	0.341	1.050	2.425	0.975	-1.099	0.025	0.365
1.045	5.055	0.970	-1.289	0.030	0.352	1.105	6.118	0.970	-1.249	0.030	0.397	1.060	2.797	0.970	-1.368	0.030	0.427
1.053	5.879	0.965	-1.444	0.035	0.401	1.123	7.035	0.965	-1.431	0.035	0.449	1.070	3.157	0.965	-1.492	0.035	0.484
1.060	6.706	0.960	-1.699	0.040	0.449	1.140	7.972	0.960	-1.627	0.040	0.501	1.080	3.508	0.960	-1.694	0.040	0.538
1.068	7.565	0.955	-1.876	0.045	0.495	1.158	9.043	0.955	-1.839	0.045	0.550	1.090	3.872	0.955	-1.899	0.045	0.591
1.075	8.431	0.950	-2.114	0.050	0.537	1.175	10.095	0.950	-1.980	0.050	0.596	1.100	4.225	0.950	-2.088	0.050	0.644
1.083	9.308	0.945	-2.288	0.055	0.583	1.193	11.161	0.945	-2.239	0.055	0.644	1.110	4.538	0.945	-2.266	0.055	0.691
1.090	10.203	0.940	-2.575	0.060	0.625	1.210	12.233	0.940	-2.404	0.060	0.690	1.120	4.888	0.940	-2.444	0.060	0.741
1.098	11.125	0.935	-2.797	0.065	0.666	1.228	13.304	0.935	-2.595	0.065	0.735	1.130	5.209	0.935	-2.596	0.065	0.789
1.105	12.056	0.930	-3.038	0.070	0.706	1.245	14.378	0.930	-2.817	0.070	0.779	1.140	5.571	0.930	-2.854	0.070	0.835
1.113	12.985	0.925	-3.336	0.075	0.747	1.263	15.378	0.925	-3.064	0.075	0.822	1.150	5.857	0.925	-2.999	0.075	0.880
1.120	13.919	0.920	-3.590	0.080	0.787	1.280	16.501	0.920	-3.225	0.080	0.864	1.160	6.219	0.920	-3.306	0.080	0.924
1.128	14.843	0.915	-3.895	0.085	0.826	1.298	17.584	0.915	-3.522	0.085	0.905	1.170	6.556	0.915	-3.394	0.085	0.968
1.135	15.784	0.910	-4.154	0.090	0.864	1.315	18.661	0.910	-3.696	0.090	0.947	1.180	6.912	0.910	-3.703	0.090	1.009
1.143	16.648	0.905	-4.476	0.095	0.902	1.333	19.718	0.905	-3.946	0.095	0.988	1.190	7.254	0.905	-3.886	0.095	1.051
1.150	17.584	0.900	-4.745	0.100	0.939	1.350	20.771	0.900	-4.159	0.100	1.027	1.200	7.500	0.900	-4.098	0.100	1.090

extra firm tofu						firm tofu					
tension $n=5$		compression $n=5$		shear $n=5$		tension $n=5$		compression $n=7$		shear $n=7$	
λ [-]	P_{11} [kPa]	λ [-]	P_{11} [kPa]	γ [-]	P_{12} [kPa]	λ [-]	P_{11} [kPa]	λ [-]	P_{11} [kPa]	γ [-]	P_{12} [kPa]
1.000	0.000	1.000	0.000	0.000	0.000	1.000	0.000	1.000	0.000	0.000	0.000
1.005	0.230	0.995	-0.214	0.005	0.063	1.008	0.389	0.995	-0.224	0.005	0.056
1.010	0.448	0.990	-0.335	0.010	0.115	1.015	0.685	0.990	-0.422	0.010	0.105
1.015	0.643	0.985	-0.419	0.015	0.164	1.023	0.927	0.985	-0.582	0.015	0.148
1.020	0.839	0.980	-0.593	0.020	0.208	1.030	1.146	0.980	-0.774	0.020	0.186
1.025	1.021	0.975	-0.649	0.025	0.251	1.038	1.345	0.975	-0.934	0.025	0.226
1.030	1.195	0.970	-0.808	0.030	0.290	1.045	1.536	0.970	-1.039	0.030	0.263
1.035	1.368	0.965	-0.856	0.035	0.329	1.053	1.720	0.965	-1.219	0.035	0.299
1.040	1.530	0.960	-1.059	0.040	0.366	1.060	1.892	0.960	-1.320	0.040	0.336
1.045	1.690	0.955	-1.122	0.045	0.403	1.068	2.061	0.955	-1.463	0.045	0.367
1.050	1.841	0.950	-1.307	0.050	0.435	1.075	2.234	0.950	-1.609	0.050	0.403
1.055	1.991	0.945	-1.344	0.055	0.471	1.083	2.395	0.945	-1.721	0.055	0.434
1.060	2.133	0.940	-1.460	0.060	0.504	1.090	2.546	0.940	-1.840	0.060	0.464
1.065	2.272	0.935	-1.563	0.065	0.537	1.098	2.692	0.935	-1.992	0.065	0.495
1.070	2.407	0.930	-1.646	0.070	0.568	1.105	2.829	0.930	-2.095	0.070	0.526
1.075	2.543	0.925	-1.796	0.075	0.599	1.113	2.967	0.925	-2.279	0.075	0.556
1.080	2.678	0.920	-1.930	0.080	0.629	1.120	3.102	0.920	-2.365	0.080	0.583
1.085	2.799	0.915	-2.073	0.085	0.659	1.128	3.228	0.915	-2.553	0.085	0.611
1.090	2.930	0.910	-2.144	0.090	0.688	1.135	3.339	0.910	-2.627	0.090	0.639
1.095	3.043	0.905	-2.279	0.095	0.717	1.143	3.449	0.905	-2.797	0.095	0.666
1.100	3.167	0.900	-2.469	0.100	0.745	1.150	3.545	0.900	-2.876	0.100	0.693

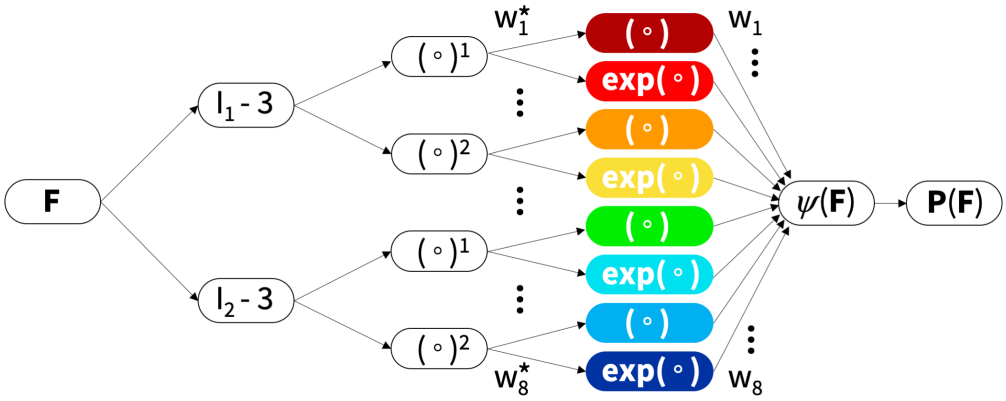

Fig. 6 Constitutive neural network. Isotropic, perfectly incompressible constitutive artificial neural network with two hidden layers and eight terms. The network takes the deformation gradient $\boldsymbol{F}$ as input and calculates its first and second invariant terms, $[I_1 - 3]$ and $[I_2 - 3]$. The first layer generates powers of these invariants, $(\circ)^1$ and $(\circ)^2$, and the second layer applies the identity and the exponential function to these powers, $(\circ)$ and $\exp(\circ)$. The strain energy function $\psi(\boldsymbol{F})$ is a sum of the resulting eight terms. Its derivative defines the Piola stress, $\partial\psi(\boldsymbol{F})/\partial\boldsymbol{F}$, whose components, P_{11} or P_{12}, enter the loss function to minimize the error with respect to the tension, compression, and shear data. By minimizing the loss function, the network trains its weights $\boldsymbol{w}$ and $\boldsymbol{w}^*$ and discovers the best model and parameters to explain the experimental data.

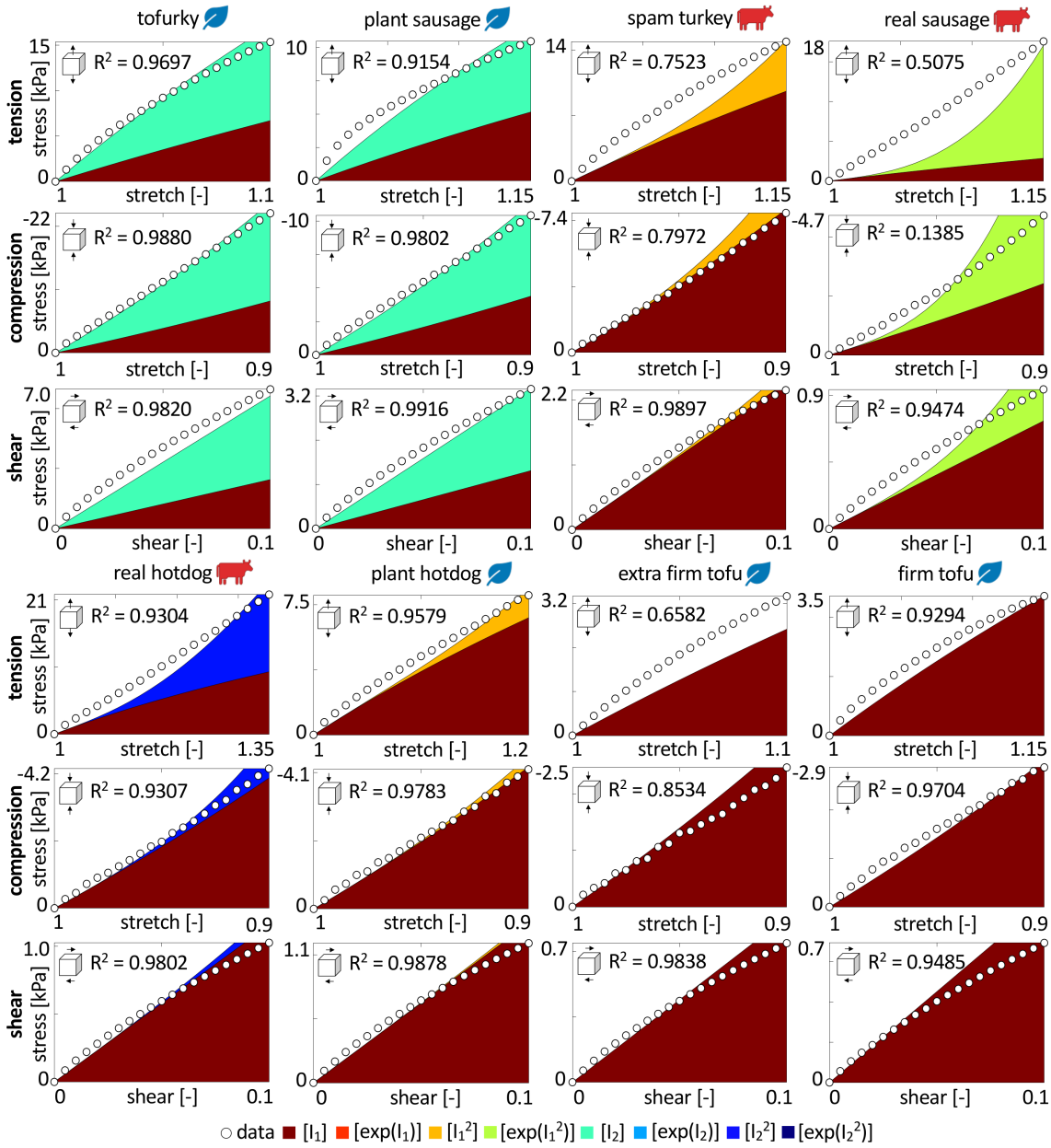

Fig. 7 Stress as a function of stretch or shear strain for the best-in-class two-term model. We train the constitutive neural network in Figure 6 simultaneously with the tension, compression, and shear data from Table 2, and apply L_0-regularization to reduce the number of terms to two according to Table 1 and Figure 3. The color-coded regions designate the contributions of the eight model terms to the stress function according to Figure 6. The coefficients of determination R^2 indicate the goodness of fit.

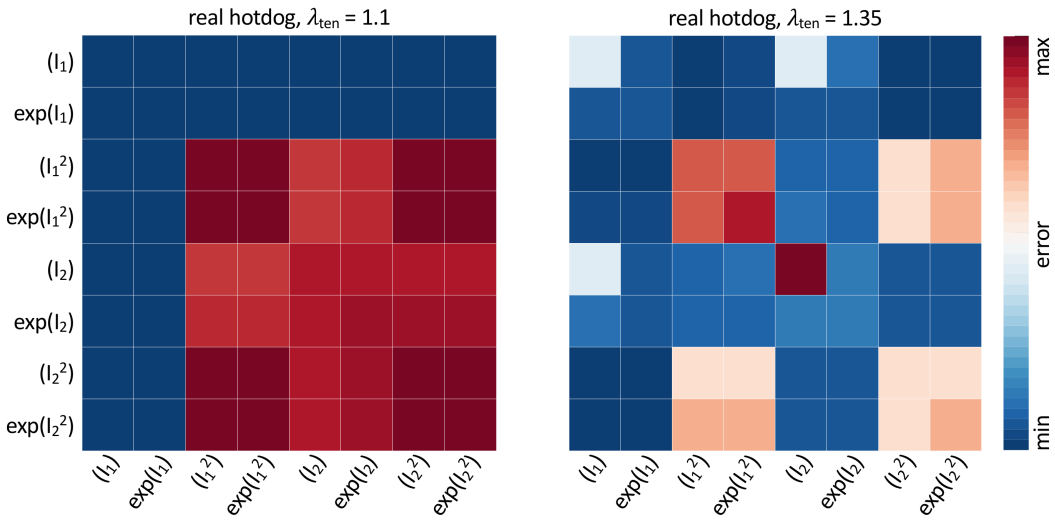

Fig. 8 Model discovery for real hotdog. Discovered one-term models, on the diagonal, and two-term models, off-diagonal, using tensile stretches up to 10% versus up to the peak stress of 35%. All models are made up of eight functional building blocks: linear, exponential linear, quadratic, and exponential quadratic terms of the first and second strain invariants I_1 and I_2. The color code indicates the quality of fit to the tension, compression, and shear data from Table 2 in the Extended Data, ranging from dark blue, best fit, to dark red, worst fit. The larger stretch range of 35% provides a clearer distinction of the quality of fit for the individual models.